Performance Analysis of Suspension Force and Torque in an IBPMSM with V-shape PMs for Flywheel Batteries

Xiaodong Sun[1], Bokai Su[1], Shaohua Wang[1], Zebin Yang[2], Gang Lei[3], Jianguo Zhu[3], and Youguang Guo[3]

[1] School of Automobile and Traffic Engineering, Jiangsu University, Zhenjiang 212013, China
[2] School of Electrical and Information Engineering, Jiangsu University, Zhenjiang 212013, China
[3] School of Electrical and Data Engineering, University of Technology, Sydney, Sydney, NSW 2007, Australia

Due to the advantages such as high energy density, high power density, high cyclic-life, and environmentally friendly, flywheel have the potential to solve the problem of energy storage. In order to improve the torque density and suspension performance of bearingless synchronous permanent magnet synchronous motors (BPMSMs), a novel rotor structure with V-shape permanent magnets (PM) is designed in this paper. Furthermore, the IBPMSM with V-shape PM which used for flywheel batteries of electric vehicles (EVs) is researched in detail. Especially, the influence of geometrical parameters of V-shape PM on suspension force and electromagnetic torque is investigated. Moreover, the corresponding static electronic magnetic characteristics including inductances, electromagnetic torque is also studied. The finite-element method (FEM) is employed to evaluate the theoretical analysis of the proposed IBPMSM. In addition, the optimized motor is validated to have good suspension performance by some experiments.

***Index Terms*—Bearingless motor, flywheel battery, V-shape PM, suspension force, electrical magnetic characteristic.**

I. Introduction

With the development of society and economy, environment deterioration and energy shortage are getting more and more concerns. Comparing with the traditional vehicles, electric vehicles (EVs) have advantages including low emissions, high energy conversion efficiency and multiple sources, and they are considered as an important way to deal with environment deterioration and energy shortage. As one of key techniques of EVs, the power battery technique is extremely important. Comparing with the conventional chemical battery, the flywheel battery has relative advantages, such as maintenance free, high energy density, high power density, rapid charge and discharge, high cyclic-life and environmentally friendly [1], [2]. The bearingless permanent magnet synchronous machine (BPMSM) with the advantages of high efficiency, high power density, high power factor and friction-free is favorable for the flywheel battery [3]-[5]. In addition, the interior BPMSMs (IBPMSMs) generating both electromagnetic torque and reluctance torque can increase power density of motors further [6].

In this paper, the structure and feature of proposed bearingless motor is introduced firstly in Section II. In Section III, the influence of V-shape PMs geometrical parameters on suspension force will be investigated. Then, the electromagnetic performance, such as torques and inductances are analyzed in following Section IV. Furthermore, the experimental platform of the BPMSM is illustrated, and some reliable suspension control experiments are made in Section V. Finally, Section VI concludes the paper.

Manuscript received March 5, 2018; revised April 9, 2018; accepted April 11, 2018. Corresponding author: S. Wang (e-mail: wsh@ujs.edu.cn)

Color versions of one or more of the figures in this paper are available online at http://ieeexplore.ieee.org.

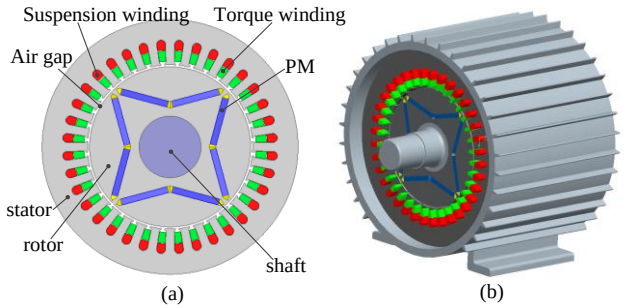

Fig. 1. Proposed bearingless machine. (a) Front view. (b) Side view.

II. Structure and Features

Fig. 1 illustrates the proposed IBPMSM with V-shape PMs. From the front view, it can be seen that the proposed motor has a similar structure with permanent magnet synchronous machine (PMSM), but the difference is the stator houses the torque and the suspension windings which fulfilled [7]

$$\begin{cases} P_S = P_T \pm 1 \\ \omega_S = \omega_T \end{cases} \tag{1}$$

where P_T is the pole-pair number of the torque winding, ω_T is the current frequency of torque winding, P_S is the pole-pair number of the torque winding, and ω_S is the current frequency of suspension winding.

The suspension force generation can be seen form Fig 2. Take one phase suspension winding and torque winding to describe the suspension principle. When the rotor is in the center location, the symmetric four-pole magnetic field Ψ_4 is generated by torque windings A and PMs. If the suspension windings is not excited, there is no suspension force generated because of Ψ_4 is balanced. When X phase is excited, the six-pole magnetic field Ψ_6 is generated by suspension windings, which together with Ψ_4 strengthen the magnetic field along the x-axis positive directions. Therefore, the air gap flux density at right is larger than left, which will generate a suspension force F_x along the x-axis positive direction. In contrast, the suspension force F_x along the x-axis negative directions will be generated if

providing reverse current. Similarly, the suspension force along the y-axis F_y will generate when the next phase suspension winding is excited.

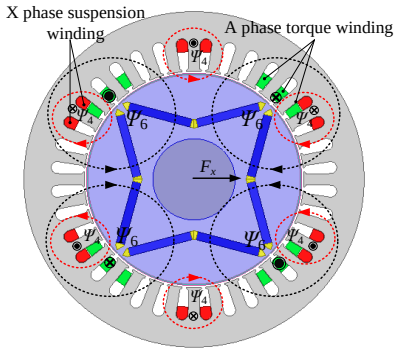

Fig. 2. Schematic diagram of the BPMSM

III. Influence of PM Geometrical Parameters on Suspension Force

The geometry parameter of PMs has important influence on performance of research motors. In this part, the geometry parameters including angle between two PMs A and the number of segments N are optimized for improving the suspension performances [8]-[12].

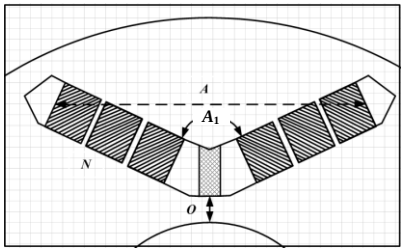

Fig. 3. Key geometrical parameters of the V-shape PM motor.

A. Suspension Force

According to the Maxwell tensor method, the suspension force model can be built, and the Maxwell force acting on the rotor surface can be expressed as

$$dF_p = \frac{B^2(\varphi,t)\mathrm{d}S}{2\mu_0} \tag{2}$$

where $B(\varphi, t)$ is airgap flux density, μ_0 is the permeability in the vacuum, S is rotor surface area.

The suspension force F_p can be decomposed into two forces, one in the x direction and one in the y direction

$$F_p = \sqrt{F_x^2 + F_y^2} \tag{3}$$

where F_x and F_y are suspension forces along x- and y-axes, respectively, and they can be written as

$$\begin{cases} F_x = k_\alpha I_S I_{PM} \cos(\theta_M - \theta_S) + k_b x \\ F_y = k_\alpha I_S I_{PM} \sin(\theta_M - \theta_S) + k_b y \end{cases} \tag{4}$$

where $k_\alpha = \dfrac{3lr\mu_0 N_S N_M k_{dS} k_{dM}}{4\pi\delta_0^2}$, $k_b = \dfrac{9\mu_0 lr N_M^2 I_{PM}^2 k_{dM}^2}{8\pi\delta_0^3}$, l is the effective rotor length, r is the rotor outer surface radius, μ_0 is the permeability in the vacuum, N_S and N_M are the coils number of suspension windings and coils number of torque windings in per phase, respectively, k_{dM} and k_{dS} are the torque windings and suspension windings stacking coefficient respectively, δ_0 is the airgap length when rotor eccentricity is not existing, I_S is suspension winding current and I_{PM} is the equivalent current of PM, θ_M and θ_S are the initial angle of torque winding current and initial angle of suspension winding current, respectively.

B. Angle Between Two PMs-A_1

It is not so easy to determine the angle between two PMs since there is currently no definite rule to choosing it. As shown in Fig. 3, the angle can be determined by parameters A or A_1, and it is usually determined according to the experiments. In this pepper, the parameter A_1 is represented the angle between two PMs of one pole. Specifically, the parameter O is kept as constant, and the angle will changed according A_1. Then the performance of suspension force and electromagnetic torque are obtained by using finite-element method (FEM). Fig. 4(a) shows the suspension force with different A_1. It can be seen that the angle between two PMs has a little influence on the amplitude of suspension. However, with the angle increasing, the standard deviation of suspension force decreases, and the stability of suspension force can be improved.

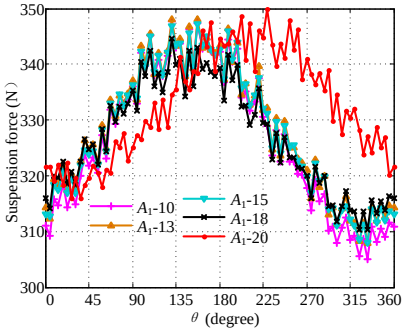

(a)

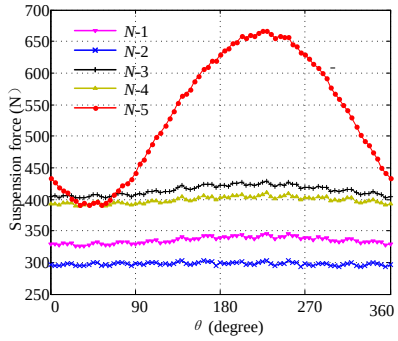

(b)

Fig. 4. Suspension force with different geometrical parameters. (a) Angle-A_1. (b) Number of segments-N.

TABLE I
Electromagnetic Torque

Angle(degree)	Average torque(N/m)
10	5.318
13	5.305
15	5.292
18	5.286
20	5.27

Table I and II show the eclectromagnetic torque performance when torque winding current is 3A with different A_1 and N,

respectively. From Table I, it can be seen that with A_1 increasing, the average torque decrease slightly.

C. Number of Segments-N

The suspension forces of the proposed IBPMSM with different N are shown in Fig. 4(b), in which the segment gaps of PM is 0.5mm and the volume of PMs is fixed. We can see from Fig. 4(b) that the N has a significant influence on amplitude of suspension force. The large fluctuation of the suspension force occurs when N is equal to 5, and the suspension force is biggest when N is equal to 3.

TABLE II
ELECTROMAGNETIC TORQUE

Segments(degree)	Average torque(N/m)
1	4.928
2	4.615
3	4.563
4	4.362
5	4.146

According to Table II, it can be seen that with the N increasing, the average torque decrease.

IV. ELECTRICAL MAGNETIC CHARACTERISTIC

Considering rotor strength and complex of process, two geometrical parameters are A_1=20 and N=3. The corresponding results of torque and the inductance characteristics are calculated with FEM and shown in Figs. 5 and 6, respectively.

A. Inductance

The inductance is one of the important technical parameters for the proposed motor, and it will have an important effect on radial suspension forces and output power. The d-axis inductance L_d and q-axis L_q can be calculated based on the three phase inductance according to

$$L(d,q,0) = C_{3/2} L(a,b,c) C_{3/2}^{T} \tag{5}$$

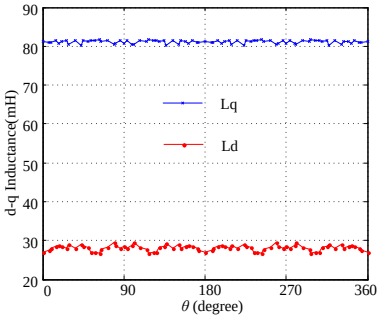

Fig. 5. d-q axis inductance.

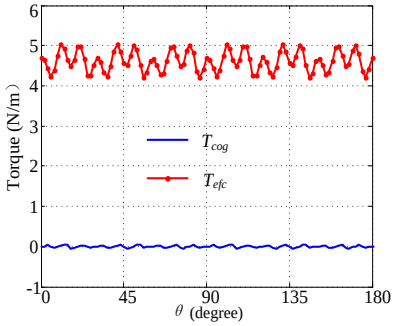

Fig. 6. Torque characteristics.

Fig. 5 shows the inductance in d-q axis, and it can be seen that the proposed motor has a large diffidence in d-q axis inductance, which can provide more reluctance torque.

B. Torque

Due to the interaction between the PMs and slotted armature lamination, the cogging torque is inevitably existed in slotted PM motors, and it may cause noise and vibration, and also influence the control precision. Fig. 6 shows the electromagnetic torque performance including electromagnetic torque T_{ele} and cogging torque T_{cog} in half cycle. As shown, the magnitude of cogging torque in proposed motors is less than 0.05% that of the electromagnetic torque. Furthermore, the cogging torque only causes the torque ripple and has no influence on value of electromagnetic torque.

V. EXPERIMENT RESEARCH

Aiming for the IBPMSMs with V-shape PM, digital control experimental equipment is developed, and reliable suspension control experiments are made.

The experimental platform of the IBPMSM is illustrated in Fig. 7, and it mainly includes hardware system of controller based control chop DSP TMS320F2812, software system compiled by Code Composer Studio (CCS), prototype, load and various sensors. In order to verify the suspension force, the static suspension experiments and suspension operation experiments are carried out in this study.

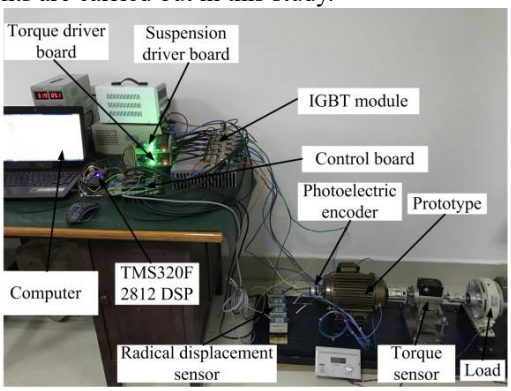

Fig. 7. Experimental platform of the BPMSM

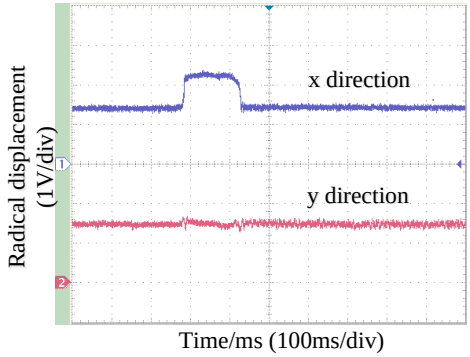

Fig. 8. Radial displacement waveforms in steady state

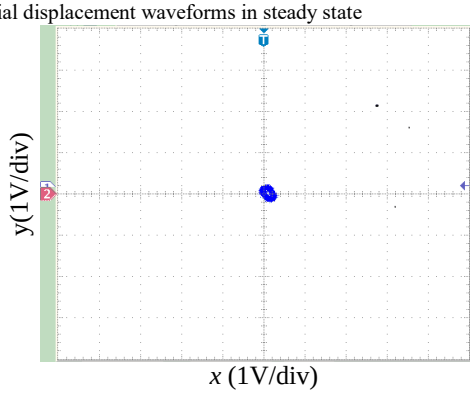

Fig. 9. Relation between radial displacement in x direction and y direction

The static suspension experiment result is shown in Fig. 8. At this point, the rotor does not rotate, and the function of the IBPMSM is just like a magnetic bearing. The rotor radial displacement waveform in disturbance working condition is shown in left side of Fig. 8, and the perturbation is set for 10N. It can be seen that when a perturbation is applied to x-axis, the radial displacement signal in x direction fluctuates greatly, after 12 ms, it can be recovered from fluctuation. Although the radial displacement signal in y direction has some fluctuations, it is a slightly fluctuation.

According to the control design, the output displacement voltage signal is about 1.5V when the rotor is located in the center position. As shown in right side of Fig 8, the waveforms of radial displacement fluctuate across the 1.5V, and the fluctuation range is within 0.15 V, that is 50 μm.

The suspension operation experiment result is shown in Fig. 9, and the rotor is rotated with suspension in this point. It can be seen from Fig. 9 that the total displacement range of the rotor vibration amplitude in the in x axis or y axis direction is approximately from -0.2V to 0.3V, that is -60μm to 100μm.

VI. Conclusion

An IBPMSM with V-shape PMs used for EVs flywheel battery is proposed in this paper. The influences of two geometrical parameters on performances of suspension force and torque are investigated The performance are sensitive to those geometrical parameters The angle between two PMs influences the stability of suspension force, and the number of segments influences the amplitude of suspension force. Furthermore, according to electrical magnetic characteristic, the proposed motor can also provide large reluctance torque and low cogging torque. The experiment results show that the control system of optimized BPMSM with V-shape PMs can realize the stable suspension operation.

Acknowledgement

This work was supported by the National Natural Science Foundation of China under Projects 51475214, 51475213, and 51305170, the Natural Science Foundation of Jiangsu Province of China under Projects BK20170071, the Key Project of Natural Science Foundation of Jiangsu Higher Education Institutions under Project 17KJA460005, the Six Categories Talent Peak of Jiangsu Province under Projects 2015-XNYQC-003 and 2014-ZBZZ-017, the “333 project” of Jiangsu Province under Project BRA2017441, the Zhenjiang Key Research and Development Project under Project GY2016003, and the Priority Academic Program Development of Jiangsu Higher Education Institutions (PAPD).

References

[1] T. Zhang, X. Liu, L. Mo, X. Ye, W. Ni, W. Ding, J. Huang, and X. Wang, “Modeling and analysis of hybrid permanent magnet type bearingless motor,” *IEEE Trans. Magn*, Vol. 54, no. 3, Mar. 2018, Art. no. 8102804.

[2] B. Han, S. Zheng, Y. Le, and S. Xu, “Design optimization of a novel heteropolar radial hybrid magnetic bearing using magnetic circuit model,” *IEEE Trans. Magn*, vol. 54, no. 3, Mar. 2018, Art. no. 8201105.

[3] X. Sun, Z. Shi, L. Chen, and Z. Yang, “Internal model control for a bearingless permanent magnet synchronous motor based on inverse system method,” *IEEE Trans. Energy Convers*, vol. 31, no. 4, pp. 1539-1548, Dec. 2016.

[4] X. Sun, L. Chen, H. Jiang, Z. Yang, J. Chen, and W. Zhang. “High-performance control for a bearingless permanent magnet synchronous motor using neural network inverse scheme plus internal model controllers,” *IEEE Trans. Ind. Electron*, vol. 63, no. 6, pp 3479-3488, Jun. 2016.

[5] X. Sun, B. Su, L. Chen, Z. Yang, X. Xu, and Z. Shi, “Precise control of a four degree-of-freedom permanent magnet biased active magnetic bearing system in a magnetically suspended direct-driven spindle using neural network inverse scheme,” *Mech Syst Signal Pr*, vol. 88, pp. 36-48, May. 2017.

[6] A. Tessarolo, M. Mezzarobba, and R. Menis, “Modeling, analysis, and testing of a novel spoke-type interior permanent magnet motor with improved flux weakening capability,” *IEEE Trans. Magn*, vol. 51, no. 4, pp. 1-10, Apr. 2015.

[7] X. Sun, L. Chen, and Z. Yang, “Overview of bearingless permanent-magnet synchronous motors,” *IEEE Trans. Ind. Electron*, vol. 60, no. 12, pp. 5528-5538, Dec. 2013.

[8] S. Xu, X. Liu, and Y. Le, “Electromagnetic design of a high-speed solid cylindrical permanent-magnet motor equipped with active magnetic bearings,” *IEEE Trans. Magn*, vol. 53, no. 8, Aug. 2017, Art. no. 8203715.

[9] G. Lei, J. Zhu, Y. Guo, C. Liu, and B. Ma, “A review of design optimization methods for electrical machines,” *Energies*, vol. 10, no. 12, Dec. 2017, Art.no. 1962.

[10] D. Wang, X. Du; D. Zhang, and X. Wang, “Design, optimization, and prototyping of segmental-type linear switched-reluctance motor with a toroidally wound mover for vertical propulsion application,” *IEEE Trans. Ind. Electron*, vol. 65, no. 2, pp. 1865-1874, Aug. 2018.

[11] G. Lei, J. Zhu, and Y Guo, *Multidisciplinary design optimisation methods for electrical machines and drive systems*, Springer-Verlag Berlin Heidelberg, 2016.

[12] D. Wang; C. Shao, and X. Wang, “Performance analysis and design optimization of an annular winding bilateral linear switch reluctance machine for low cost linear applications,” *IEEE Trans. Appl. Supercond*, vol. 26, no. 7, Oct. 2016, Art. no. 0609705.